

An Artificial Chameleon Skin for Dynamic Thermoregulation

Jiahui Liu, Liqian Zhu, Shuyuan Gao, Yuanyuan Liu, Shengjie Wang, and Yongqing Xia*

Solar radiation is the major energy source for most living creatures, and some creatures change their skin colors responding to energy demands. Inspired by the chameleons that live in the desert of Namibia, which can regulate body temperature by changing skin colors between black and white, a patterned hydrogel film with self-thermoregulation ability is reported in this work. The film consists of two parts: a light-responsive black part and a stretchable white part. The black part is made of thermoresponsive poly(*N*-isopropylacrylamide) hydrogel with polydopamine (PDA) nanoparticles, and the white part is made of stretchable polyacrylamide hydrogel with polystyrene (PS) nanoparticles. At low temperature and low light irradiation, the black part dominates the film, and the embedded melanin-like PDA nanoparticles adsorb light and convert it to heat, thus reaching an active body temperature. At high temperature and strong light irradiation, the black part shrinks, which in turn stretches the white part to dominate the film, and more light is reflected by guanine crystals-like PS nanoparticles, thus protecting body temperature from rising. The combination of the thermoresponsive black hydrogel and stretchable white hydrogel provides an evolutionary novelty that can control the solar lights for dynamic thermoregulation.

1. Introduction

With the rapid development of technology, the consumption of energy increased continuously and has led to a serious environmental crisis.^[1–3] However, in nature, many creatures such as morpho butterflies,^[4,5] chameleons,^[6,7] silver ants,^[8,9] and other terrestrial ectotherms^[10–13] can remain their body temperature by spectral controlling. Chameleons that live in the desert of


Namibia can adapt to environmental temperatures by changing their body colors between black and white. Their skins are dark in the morning to adsorb more solar radiation to reach an active body temperature, and then become white at hot noon to reflect solar energy to protect body temperature (Figure 1a). This physiological process is accomplished by moving melanin particles up and down around the thick layer of D-iridophores, which can reflect infrared light for thermal protection (Figure 1b).^[14,15]

Inspired by natural creatures, a wide variety of materials with specific functionalities such as high solar radiation absorption (e.g., carbon materials,^[16–21] noble metal nanoparticles,^[22,23] and structural materials^[24–27]) or reflection (whiteness^[28,29] and metals^[30,31]) were reported. However, it is still a great challenge to design materials with both thermal adsorption and reflection functions to adapt to the dynamic surrounding environments. Up to date, most dynamic thermoregulatory materials were achieved by

changing from transparent to opaque with temperature varies. Besides VO₂, the most widely used traditional thermoregulatory material,^[32–34] thermoresponsive hydrogels and microgels were also reported for thermoregulation.^[35–37]

Here, we designed a light-responsive artificial chameleon skin that can sense temperature and alter its color expression by emulating the self-thermoregulation mechanism of Namibia chameleons. The strategy is to prepare patterned film with dynamic area change of solar energy adsorption and reflection. The artificial skin consists of two parts: the thermoresponsive black part for light harvesting, and the stretchable white part for light reflection (Figure 1c). The black part is made of poly(*N*-isopropylacrylamide) (PNIPAM) hydrogel embedded with polydopamine (PDA) nanoparticles, which can adsorb light and convert it to heat; the white part is made of stretchable polyacrylamide (PAM) hydrogel embedded with polystyrene (PS) colloids, which reflect light like large guanine crystals. At low light irradiation and low temperature, the dark film dominates the surface, and the PDA nanoparticles adsorb the weak light and generate heat to increase body temperature. At high light irradiation, when the temperature reaches the volume phase transition temperature (VPTT) of the PNIPAM hydrogel, the dark part begins to shrink, which in turn stretches the white PAM film to spread, and then the white part dominates the film and more

J. Liu, L. Zhu, S. Gao, Y. Liu, S. Wang, Y. Xia
Department of Biological and Bioenergy Chemical Engineering
College of Chemical Engineering
China University of Petroleum (East China)
Qingdao 266580, China
E-mail: xiayq@upc.edu.cn

 The ORCID identification number(s) for the author(s) of this article can be found under <https://doi.org/10.1002/admi.202202124>.

© 2023 The Authors. Advanced Materials Interfaces published by Wiley-VCH GmbH. This is an open access article under the terms of the Creative Commons Attribution License, which permits use, distribution and reproduction in any medium, provided the original work is properly cited.

DOI: 10.1002/admi.202202124

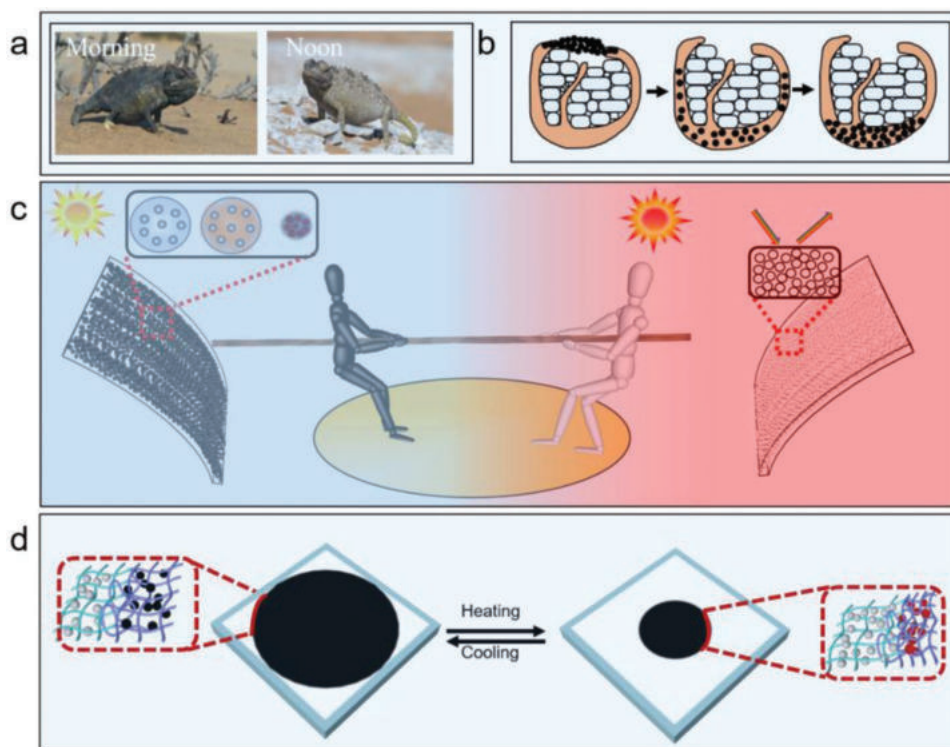


Figure 1. a) The skin color of Namibia chameleon in the morning and at noon (Chameleon images from xsj.699pic.com, a royalty-free website). b) The corresponding melanin granules move up and down through the microtubules in the dermal. c) The illustration of the heat absorption and reflection of the thermoregulation skin, the black for heat adsorption and photothermal conversion, and the white part for heat reflection. d) The illustration of the designed artificial skin and its dynamic thermoregulation property is achieved by the shrinkage of the black part and expansion of the white part.

light energy is reflected, thus the body temperature is protected from rising (Figure 1d). The combination of the functional two parts provides an evolutionary novelty that can precisely control the spectrum for thermal regulation and may open a new application opportunity for dynamic thermoregulation.

2. Results and Discussion

Although chameleons primarily change color for camouflage in the wild, their color change may also aid in thermoregulation,^[38,39] such as chameleons living in the desert. The observed color change provides a thermoregulatory advantage because it increases the absorption of solar radiation at low temperatures and decreases absorption at high temperatures. Since the physiological function of the chameleon is difficult to mimic, a model was built to mimic the skin color area change in this work.

2.1. The Dark Film for Photothermal Conversion

Efficient solar harvest is vital for living organisms to survive in harsh environments, and natural pigments such as melanin, which has unique solar–thermal properties play a variety of key roles in the thermoregulation of ectotherms. In recent years, melanin has attracted much interest for its outstanding properties, such as anti-ultraviolet (UV),^[40,41] metal chelating,^[42] free radical scavenging,^[43,44] and thermoregulation.^[45,46] PDA, the most

common type of synthetic melanin, has been revealed that its physicochemical properties are generally similar to those of natural melanins, thus PDA has been used as photoprotectors, antioxidants,^[43] semiconductors,^[47] and biomedical materials.^[48,49] Moreover, the strong adhesive^[50–52] and light absorption^[40,49] properties of PDA are beneficial for interface engineering.

The PDA nanoparticles in this work were synthesized via oxidation and a self-polymerization procedure. Transmission electron microscope (TEM) image and dynamic light scattering (DLS) results showed that the size of the PDA nanoparticles is around 285 nm (Figure S1a,b, Supporting Information). The light absorption ability and solar–thermal effect of the prepared PDA nanoparticles were studied. **Figure 2a** shows the PDA nanoparticles have strong adsorption in the UV–vis range. **Figure 2b** exhibits the temperature elevation of PDA nanoparticle solution with different concentrations under one equivalent solar irradiation (100 mW cm^{-2}). When the concentration of PDA falls within a range of $0\text{--}5 \text{ mg mL}^{-1}$, the solution temperature and photothermal conversion efficiency increase with increasing PDA concentrations. However, the increment of temperature is nonlinear to the PDA concentration, and the photothermal efficiency of PDA at 4 mg mL^{-1} was very close to that at 5 mg mL^{-1} . The reason is a high concentration of PDA could reduce light penetration.^[53] Thus, 5 mg mL^{-1} PDA is adopted in our work. The temperature of the PDA solution with 5 mg mL^{-1} increased to $50 \text{ }^\circ\text{C}$ within 15 min and has risen by $30 \text{ }^\circ\text{C}$, while the temperature of pure water has risen by $10 \text{ }^\circ\text{C}$ at the same time. The solar–thermal conversion efficiency (η)

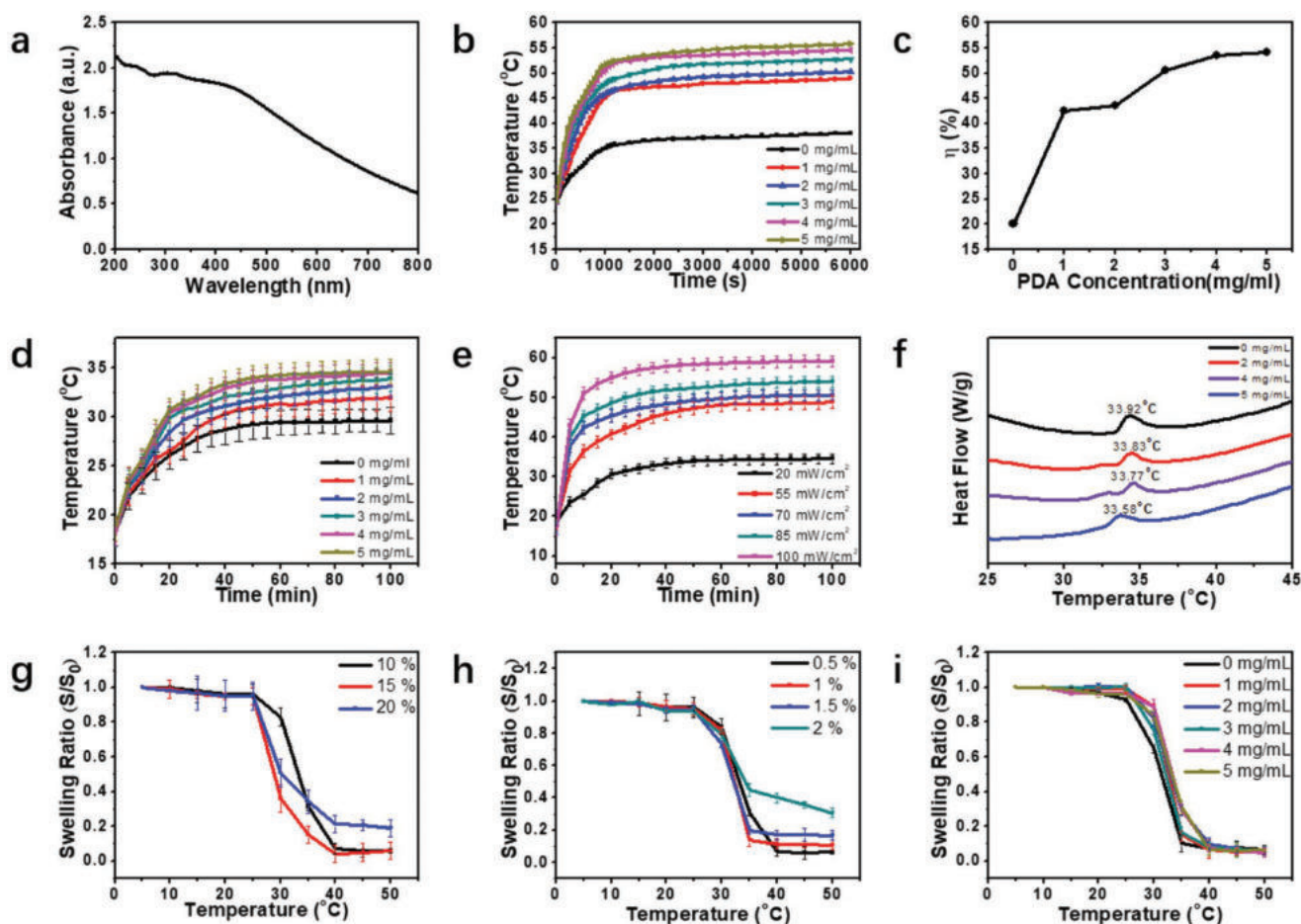


Figure 2. a) UV-vis spectra of PDA ranging from 200 to 800 nm. b) Temperature elevations of PDA at different concentrations under 1-sun solar irradiation (100 mW cm⁻²). c) The plot of solar-thermal conversion efficiency (η) versus concentration of the xenon concentration of PDA nanoparticles. d) The photothermal response of the black film with different PDA concentrations under the irradiation of the xenon lamp (20 mW cm⁻²). e) The photothermal response of the black film with different irradiation power of the xenon lamp with 5 mg mL⁻¹ PDA. f) The effect of PDA concentration on the VPTT of the PNIPAM hydrogel. g) The effect of monomer concentration on the thermoresponsive of the PNIPAM hydrogel. h) The effect of cross-linking degree on the thermoresponsive of the PNIPAM hydrogel. i) The effect of PDA concentration on the thermoresponsive of the PNIPAM hydrogel. The data were presented as the mean \pm SD ($n = 3$).

of the solution with different PDA concentrations can be calculated through the linear time data versus $\ln(1 - \theta)$ (Figure S2, Supporting Information). Figure 2c shows the solar-thermal conversion efficiency (η) of the solution increased from 40% to 55% with the increasing concentration of PDA increasing from 1 to 5 mg mL⁻¹, similar to previous reports.^[46,54]

When the PDA nanoparticles were mixed with the PNIPAM pregel solution, they can be entrapped by the polymer matrix (Figure S3, Supporting Information, red arrow indicated). Under the irradiation of 20 mW cm⁻², the surface temperature of the film increased with the PDA concentration increasing, and the increasing amplitude was significantly greater when the PDA concentration was beyond 3 mg mL⁻¹ (Figure 2d). The surface temperature also depends much on the irradiation power, higher irradiation power resulted in higher surface temperature. Even under lower irradiation power (20 mW cm⁻², like the heat of the sun in the morning), the surface temperature can reach 33 °C in 20 min from 16 °C, which is high enough for ectotherms to keep active. Moreover, the addition

of the PDA particles had no obvious effect on the VPTT of the PNIPAM (Figure 2f).

The thermoresponsive of the PNIPAM hydrogel played an important role in the color change of the artificial surface. In this system, the thermoresponsive of the hydrogel mainly depended on the monomer concentration and crosslinking degree. Lower monomer or lower cross-linking degree led to high surface area shrinking (Figure 2g,h). Thus 10% monomer concentration and 0.5% crosslinking degree were adopted in this work. The effect of PDA addition on the equilibrium swelling ratio was exhibited in Figure 2i, it showed clearly that the concentration of PDA has no obvious effect on the thermoresponsiveness of the film.

2.2. The White Film for Light Reflection

Although solar light is necessary, it can also be harmful to creatures that live in high-temperature environments. Thus,

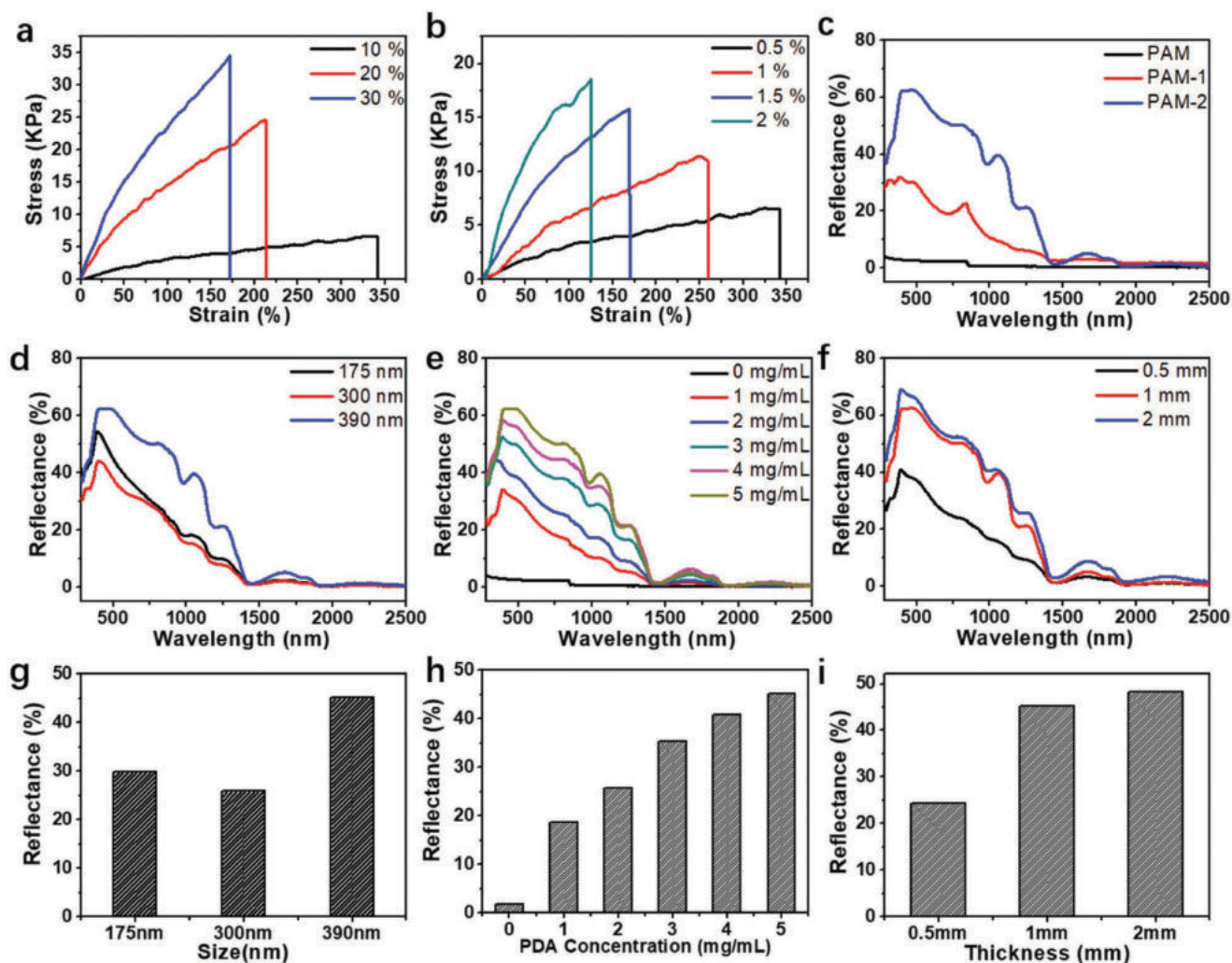


Figure 3. a) Effects of monomer concentration on the mechanical properties of the PAM hydrogels. The crosslinking degree was fixed at 0.5%. b) Effects of crosslinking degree on the mechanical properties of the PAM hydrogels. The monomer concentration was fixed at 10%. c) The reflectance spectra of the white films with PS particles by different embedding methods. d) The reflectance spectra of the white films with different PS colloid sizes. e) The reflectance spectra of the white films with different PS particles (390 nm) concentrations. f) The reflectance spectra of the white films with different thicknesses. (g), (h), and (i) are the calculated solar reflectivity of the films at the condition of (d), (e), and (f).

high reflection over the Vis-NIR band for thermal regulation is required in those circumstances. To make a temperature protection film, stretchable PAM hydrogel embedded with PS microspheres was designed to achieve this function. The PS colloids can be embedded in the hydrogel matrix (Figure S4, Supporting Information, red arrow indicated). Since the expansion of the white part is achieved by the shrinkage of the black part, we hope the white part is stretchable. The flexibility of the PAM film depended on the monomer concentration (Figure 3a) and crosslinking degree (Figure 3b). When the cross-linking degree was constant, lower monomer concentration resulted in more defects in the polymer skeleton. Thus the hydrogel exhibited macroscopic softness, with low stress and high strain. With the monomer concentration increasing, the number of the polymer chain increased, the network became more perfect and resulting in higher stress and lower strain. The effect of cross-linking degree on hydrogel stress-strain behavior was similar to monomer concentration. A higher cross-linking degree led

to more cross-linking points, which shortened the polymer chains, and resulted in higher stress with lower strain. When the monomer concentration and the cross-linking degree were 10% and 0.5%, respectively, the PAM film can be stretched to 350% with only 6.57 kPa stress. Hence, the PAM film with 10% monomer concentration and 0.5% cross-linking degree was adopted in this work.

There were two ways to make the white film with high reflectance by embedding the PS colloids into the PAM hydrogel. One was to form ordered PS colloid arrays on the PAM hydrogel film (PAM-1), and the other was mixing the particles with the pregel solution to form completely disordered colloid arrays (PAM-2). To quantify the reflectance of the films, they were measured using an integrating sphere from 300 to 2500 nm, and pure PAM film without the PS colloids (PAM-0) was used as control. The reflectance spectra (Figure 3c) showed that PAM-2 had higher reflectivity. The solar reflectivity of PAM-0 and PAM-1 was only 1.81% and 19%, respectively, while

the solar reflectivity of PAM-2 can be as high as 45.1%, more than twice the reflectivity value of PAM-1. The reason is in PAM-1, the PS colloid film remained an ordered structure and the thickness was thinner than that of the bulk PAM hydrogel, allowing most light to pass through and reflecting only a small fraction of light. In PAM-2, the PS colloids were dispersed in the whole hydrogel randomly, which resulted in a decrease in light transmittance and an increase in light scattering. Hence, the solar reflectivity of PAM-2 was higher than that of PAM-1, and PAM-2 was used for further investigation. The size of the PS colloids also affected the reflection effect. Different sizes of PS colloids can be obtained by tuning the amount of surfactant SDS (175 nm, 300 nm, and 390 nm; Figure S5, Supporting Information), and a series of PAM-2 films with different PS colloid diameters were prepared. The reflectance spectra of the PAM-2 films with different sizes of PS colloids (Figure 3d) had similar in terms of trends, but with different intensities. The calculated solar reflectivity increased from 29.9% to 45.1% as the PS diameter increased from 175 to 390 nm (Figure 3h). Compared with the films with PS colloid sizes of 175 and 300 nm, the PAM-2 film with PS colloid size of 390 nm had higher solar reflectivity, thus 390 nm PS colloids were used in this work. Reflective spectra in Figure 3e showed clearly that the reflectance intensity increased with the PS colloid concentration increasing. The calculated solar reflectivity in Figure 3i

proved that the solar reflectivity of the films increased from 18.7% to 45.1% gradually as PS colloid concentrations increased from 1 to 5 mg mL⁻¹; thus, 5 mg mL⁻¹ PS colloid was used in the further experiment. The film thickness is another crucial factor for the reflection effect. Figure 3f shows the film reflectance spectra with different film thicknesses. As the thickness of the film increased from 0.5 to 1 mm, the calculated solar reflectivity increased from 24.4% to 45.1%. However, the solar reflectivity could not increase unlimitedly with the increase of the film thickness, and the reflectivity was 48.2% when the film thickness increased to 2 mm (Figure 3j). Thus 1 mm is good enough to serve as an effective reflectance shield against strong light and reduce solar absorption.

2.3. Artificial Skin for Thermoregulation

Although many effective technical strategies have been reported to enhance the interfacial bonding of different polymer composites, the surface modification processes were complex and high cost.^[55,56] Luckily, using a mussel-inspired modifier such as dopamine probably was an effective and environmental-friendly way to enhance the interfacial bonding between polymer matrices. PDA contains both catechol and amine groups in the structure, resulting in high adhesiveness to a wide range of

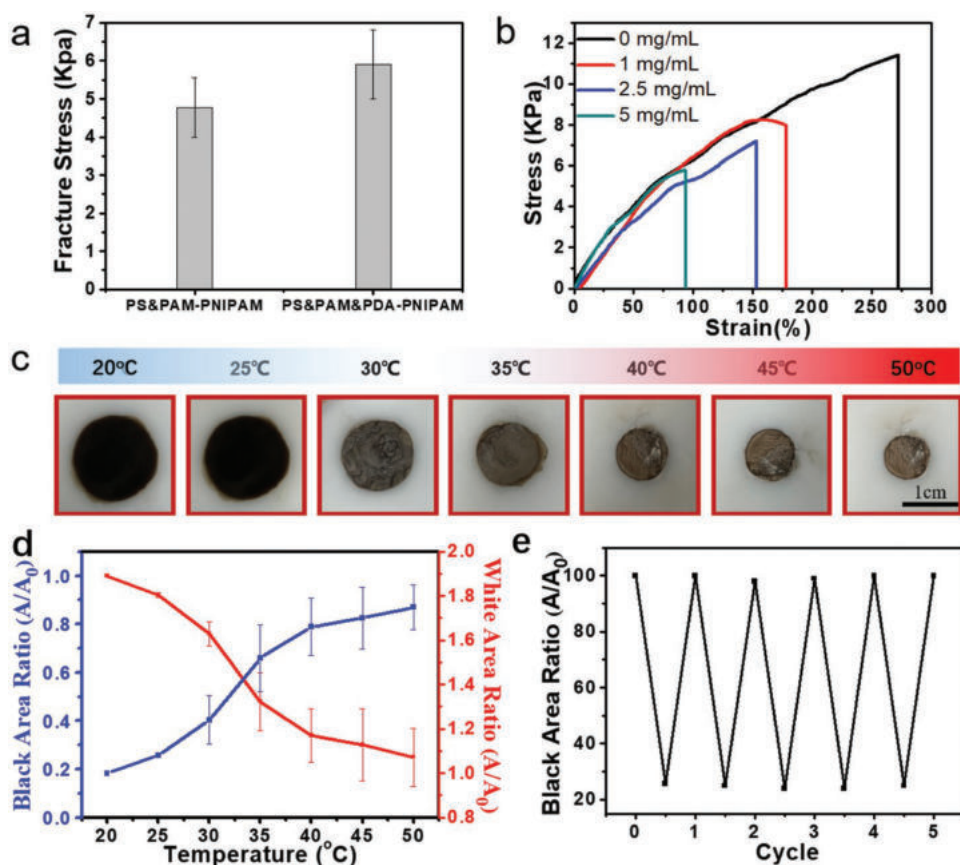


Figure 4. a) The mechanical properties of the PAM film connected with PNIPAM film with/without PDA. b) The effects of the PDA concentrations on the mechanical strength of the PNIPAM film. c) The designed white-black film changed the color area with temperature stimuli. d) Analysis of the color area change of the artificial skin at different temperatures. e) The reversibility of the artificial skin in the water environment. The data were presented as the mean \pm SD ($n = 3$).

materials.^[50,57] PDA nanoparticles in the PNIPAM hydrogel also enhanced the bonding strength with PAM hydrogel. Without PDA nanoparticles, the patterned film broke up at the interface between the PNIPAM and PAM film, and the interface bonding strength is 4.77 kPa. When the PNIPAM hydrogel containing 5 mg mL⁻¹ PDA nanoparticles, the patterned film didn't break at the interface, but at the PNIPAM film, and the strength is 5.91 kPa (Figure 4a). This means the bonding interface strength was much higher than the fracture strength of the PNIPAM film. Although the exact bonding strength between the white part and the black part was not determined, the results showed that the interfacial bonding was sufficiently large to operate the artificial skin. It's worth noting that Young's modulus of the PNIPAM hydrogel decreased with the PDA concentration increasing (Figure 4b). The reason may be a high concentration of PDA inhibited the polymerization of PNIPAM hydrogel by quenching the free radicals, resulting in an incomplete polymerization.^[58] To balance the mechanical strength and the photothermal conversion, the PNIPAM hydrogel with 5 mg mL⁻¹ PDA was adopted in this work.

Then, the black and white film was integrated to study the dynamic surface area change at different temperatures. The edges of the white film were fixed; thus, the shrinking of the black film could stretch the white film to spread. Figure 4c displays that the black part shrank, and the white part according increased with the temperature increasing. From 20 to 33 °C, the black film shrank gradually to 50% of its original area. At 40 °C, the black part shrank to 30%, and then to 22% at 50 °C. Accordingly, the white film enlarged to 180% of its original area at 50 °C (Figure 4d). More exciting, the change of the black part and the white part surface areas is reversible (Figure 4e).

To mimic the body structure (Figure 5a), the film was attached to agarose bulk hydrogel (the thickness is about 10 mm). The agarose hydrogel was used to mimic tissue engineering, thus the temperature in the agarose was determined to investigate the thermoregulation ability of the surface skin (Figure 5b). Figure 5c shows the temperature in the agarose with different films under low irradiation power (20 mW cm⁻²) and low surrounding temperature (16–17 °C). Results showed that the artificial skin with a 75% black area had the fastest

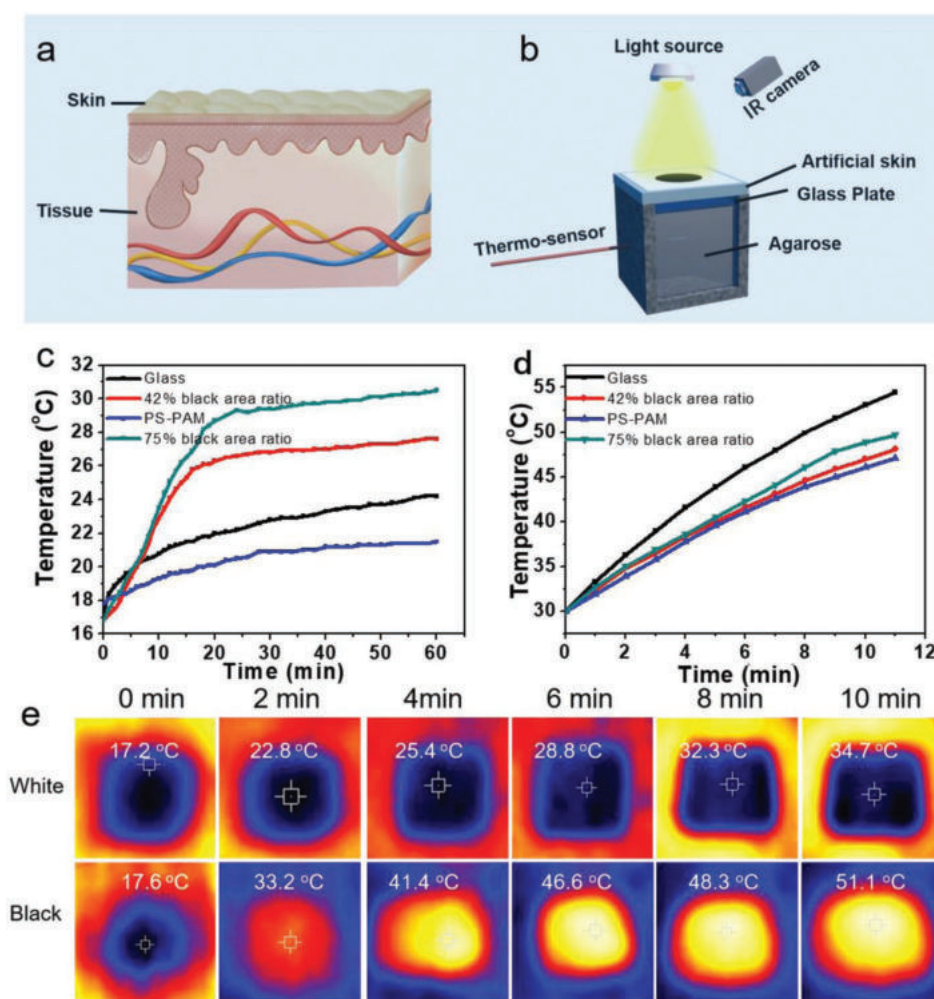


Figure 5. a) The scheme of body structure. b) The illustration of the designed artificial skin for thermoregulation. c) The temperature in agarose at 20 mW cm⁻² irradiation. d) The temperature in agarose at 150 mW cm⁻² irradiation. e) The thermal images of the white part and black part under 100 mW cm⁻² irradiation.

heating rate, achieving 30 °C in 20 min, which is high enough to keep the body active. The 42% black-white film had a faster heating rate with the highest temperature of 26 °C. The glass had a slower heating speed, and the highest temperature was only 22 °C, with PS-PAM film could only increase the temperature to 20 °C. This means the artificial can effectively convert photos to thermal even at low irradiation power.

Figure 5d shows the thermal protection of the artificial skin when the environmental temperature was 30 °C. Under high irradiation power (150 mW cm⁻², equivalent to 1.5 suns), the white PS-PAM film had the most effective thermal protection, while the glass had the worst thermal protection effect. The artificial skin with 42% and 75% black area had an obvious thermal protection effect, the temperature could reduce by 6.4 and 4.8 °C, respectively. The solar exposure (1-sun radiation) would heat the white part to 34.7 °C and the black part to 51.1 °C within 10 min (Figure 5e). Even in the air environment, the artificial skin also exhibited high reversibility (Figure S6, Supporting Information).

3. Conclusion

Combining thermoresponsive black hydrogel and stretchable white hydrogel, we prepared patterned film with self-color-area-regulation properties, which displayed thermoregulation properties under solar irradiation energy. At low solar irradiation and environmental temperature, the black PNIPAM hydrogel, which embedded PDA nanoparticles, can effectively increase the temperature from 16 to 33 °C in 20 min by photothermal conversion. At high solar irradiation and high environmental temperature, the white PAM hydrogel, which embedded PS nanoparticles, can effectively reflect the light as the dominant area, and the temperature inside the hydrogel increased slowly from 30 to 45 °C in 10 min. The thermoregulation was achieved by a change of 180% in the black-white area under temperature stimuli. Compared with the reported monofunctional materials, the photothermal conversion efficiency and radiative cooling efficiency of the artificial skin were not high. However, the artificial skin in this work showed unique thermoregulation properties, which made it have a chameleon-like function. This artificial skin opens new applications in the area of thermoregulation and switchable color display.

4. Experimental Section

Materials: Initiator (NH₄)₂S₂O₈ (APS) was purified by recrystallization. Other materials, such as styrene (St), acrylamide (Am), N,N'-methylene bisacrylamide (MBA), sodium dodecylbenzene sulfonate (SDS), dopamine hydrochloride, ammonia aqueous solution were used without further purification. All reagents were provided by sigma. The water used in this experiment was processed by the Milli-Q system (Milli-Q Advantage A10 Water System Production Unit).

Preparation of the PDA Nanoparticle: The approach to synthesizing PDA was according to a well-established method.^[59] Dopamine hydrochloride was dissolved in a mixture of deionized water and ethanol. After stirring for 10 min at room temperature, ammonia aqueous solution was then added to the above solution. After a 24 h reaction, the PDA nanoparticles were obtained by centrifugation and washed three times with deionized water.

Preparation of the Dark Hydrogel Film: A determined concentration of PDA nanoparticles was added into the PNIPAM pregel solution and mixed, then the mixture was initiated by the APS-TEMED initiator system to form the hydrogel. The swelling ratio of the hydrogel samples was obtained by optically measuring the diameter of the samples at a determined temperature by water bathing. The temperature of the black film surface under simulated sunlight (Xe lamp, CEL-HXUV300) with various power was monitored using a thermal camera (HT-02).

Solar-thermal Evaluation: Solar-thermal conversion efficiency (η) was determined as the following: Aqueous suspensions of PDA nanoparticles with different concentrations (0–5 mg mL⁻¹) were added into a quartz cuvette and illuminated vertically from the above with the solar simulator. A thermocouple probe with an accuracy of 0.1 °C was inserted into the aqueous solution perpendicular to the path of the laser. The temperature was recorded by a digital thermometer with a thermocouple probe. The solar-thermal conversion efficiency η was calculated according to the following equation^[60]

$$\eta = \frac{hS(T_{\max} - T_{\text{Surr}}) - Q_0}{I} \quad (1)$$

where h is the heat transfer coefficient (%), S is the surface area (cm²) of the container, T_{Max} and T_{Surr} (°C) are the equilibrium temperature of the test suspensions and the surrounding temperature, respectively. Q_0 is the heat yielded from the solar absorbed by the cuvette and the water. I is the effective sunlight power (mW cm⁻²) irradiated upon the suspension. Detailed calculation methods can be found in supporting information 1.

Preparation of the PS Colloids: PS colloids with various diameters were prepared using emulsion polymerization, and the colloid size was tuned by the amount of surfactant SDS. The size of the PS colloids was determined by dynamic light scattering (DLS) on a Zetasizer Nano instrument (Malvern Instruments Ltd) with the detector positioned at the scattering angle of 173°.

Preparation of the White Hydrogel Film: The white hydrogel was prepared by two different methods. One (PAM-1) is prepared by casting the PAM pregel solution onto the ordered PS colloid arrays to polymerize, thus amorphous PS colloid crystals were entrapped on the surface of the PAM hydrogel film. The other (PAM-2) is mixing the PS colloids with the PAM pregel solution completely, then the pregel was cast onto the glass slide to polymerize.

Solar-Reflectivity Evaluation: The normal reflectivity measurement of the films under light wavelengths ranging from 250 to 2500 nm was conducted on a UV-vis-NIR spectrophotometer (Shimadzu UV3600). The solar reflectivity of the prepared samples was calculated according to the equation

$$\rho_e = \frac{\sum_{\lambda=300 \text{ nm}}^{\lambda=2500 \text{ nm}} \rho_0(\lambda) S_{\lambda} \Delta\lambda}{\sum_{\lambda=2500 \text{ nm}}^{\lambda=2500 \text{ nm}} S_{\lambda} \Delta\lambda} \quad (2)$$

where ρ_e is the solar reflection of the film, $\rho_0(\lambda)$ is the direct sunlight reflection ratio, λ is the relative spectral distribution of solar radiation, and $\Delta\lambda$ is the wavelength spaces. $S_{\lambda} \Delta\lambda$ is a constant value at different wavelengths and can be obtained from ISO9050-2003.^[61]

Preparation of the Patterned Black-White Film: The patterned black-white film was prepared as follows: a square white film was prepared first, and then a circular hole was made in the middle of the square. The black hydrogel pregel solution was cast into the designed circular hole to polymerize, and then the obtained black-white film was fixed by frames to investigate its color-area change with temperature change.

Mechanical Strength Test of the Film: The mechanical strength of the samples was measured on a dynamic mechanical analyzer (HY-0580). For the black-white film, a stripe-patterned film was prepared to measure the intersurface bonding force.

Thermoregulation Evaluation: Dynamic thermoregulation experiments were carried out in a homemade artificial tissue. Agarose hydrogel was used to mimic tissue engineering. The upper surface of the

agarose hydrogel was covered by the artificial skin and the other sides were covered by blocks of PS foam to decrease thermal conduction. An automatic shutter linked with a xenon lamp (CEL-HXUV300) accurately controlled the switch of the heat source. An electronic probe thermometer was inserted into the agarose hydrogel (1 cm under the film) to measure the temperature.

Supporting Information

Supporting Information is available from the Wiley Online Library or from the author.

Acknowledgements

This work was supported by financial support from the Natural Science Foundation of Shandong Province (ZR2020MB076).

Conflict of interest

The authors declare no conflict of interest.

Data Availability Statement

The data that support the findings of this study are available in the supplementary material of this article.

Keywords

hydrogel, reflection, solar–thermal conversion, thermoregulation, thermoresponsive

Received: September 27, 2022

Revised: December 8, 2022

Published online: March 2, 2023

- [1] S. Bilgen, *Renewable Sustainable Energy Rev.* **2014**, *38*, 890.
- [2] M. A. Khan, M. Z. Khan, K. Zaman, L. Naz, *Renewable Sustainable Energy Rev.* **2014**, *29*, 336.
- [3] M. E. Bildirici, S. M. Gokmenoglu, *Renewable Sustainable Energy Rev.* **2017**, *75*, 68.
- [4] C. P. Barrera-Patino, J. D. Vollet-Filho, R. G. Teixeira-Rosa, H. P. Quiroz, A. Dussan, N. M. Inada, V. S. Bagnato, R. R. Rey-Gonzalez, *Sci. Rep.* **2020**, *10*, 5786.
- [5] Priyanka, S. K. Saini, S. Sharma, N. Singh, M. Khokhar, R. V. Nair, *J. Opt. Soc. Am. B* **2021**, *38*, 2297.
- [6] K. R. Smith, V. Cadena, J. A. Ender, W. P. Porter, M. R. Kearney, D. Stuart-Fox, *P. R. Soc. B: Biol. Sci.* **2016**, *283*, 1832.
- [7] S. V. Saenko, J. Teyssier, D. van der Marel, M. C. *BMC Biol* **2013**, *11*, 105.
- [8] N. N. Shi, C. C. Tsai, F. Camino, G. D. Bernard, N. Yu, R. Wehner, *Science* **2015**, *349*, 298.
- [9] R. Wehner, S. Wehner, *Physiol. Entomol.* **2011**, *36*, 271.
- [10] P. Vukusic, B. Hallam, J. Noyes, *Science* **2007**, *315*, 348.
- [11] D. Xie, Z. Yang, X. Liu, S. Cui, H. Zhou, T. Fan, *Soft Matter* **2019**, *15*, 4294.
- [12] S. H. Choi, S.-W. Kim, Z. Ku, M. A. Visbal-Onufrak, S.-R. Kim, K.-H. Choi, H. Ko, W. Choi, A. M. Urbas, T.-W. Goo, Y. L. Kim, *Nat. Commun.* **2018**, *9*, 452.
- [13] J. Yang, X. Zhang, X. Zhang, L. Wang, W. Feng, Q. L. *Adv. Mater.* **2021**, *33*, 2004754.
- [14] J. Teyssier, S. V. Saenko, D. van der Marel, M. C. Milinkovitch, *Nat. Commun.* **2015**, *6*, 6368.
- [15] H. Gonome, M. Nakamura, J. Okajima, S. Maruyama, *Sci. Rep.* **2018**, *8*, 1196.
- [16] K. Fu, Y. G. Yao, J. Q. Dai, L. B. Hu, *Adv. Mater.* **2017**, *29*, 1603486.
- [17] G. Ni, N. Miljkovic, H. Ghasemi, X. P. Huang, S. V. Boriskina, C. T. Lin, J. J. Wang, Y. F. Xu, M. M. Rahman, T. J. Zhang, G. Chen, *Nano Energy* **2015**, *17*, 290.
- [18] Q. Zhang, W. L. Xu, X. B. Wang, *Sci. China Mater.* **2018**, *61*, 905.
- [19] X. Zhang, Y. Yang, P. Xue, C. Valenzuela, Y. Chen, X. Yang, L. Wang, W. Feng, *Angew. Chem., Int. Ed.* **2022**, *61*, e202211030.
- [20] M. Y. Yang, Y. Y. Xu, X. Zhang, H. K. Bisoyi, P. Xue, Y. Z. Yang, X. Yang, C. Valenzuela, Y. H. Chen, L. Wang, W. Feng, Q. Li, *Adv. Funct. Mater.* **2022**, *32*, 2201884.
- [21] P. Xue, H. K. Bisoyi, Y. Chen, H. Zeng, J. Yang, X. Yang, P. Lv, X. Zhang, A. Priimagi, L. Wang, X. Xu, Q. Li, *Angew. Chem., Int. Ed.* **2021**, *60*, 3390.
- [22] A. Kumar, P. Choudhary, A. Kumar, P. H. C. Camargo, V. Krishnan, *Small* **2022**, *18*, e2101638.
- [23] F. Pini, R. Pilot, G. Ischia, S. Agnoli, V. Amendola, *ACS Appl. Mater. Interfaces* **2022**, *14*, 28924.
- [24] Y. Wang, J. Hou, Y. Huang, Y. Fu, *Int. J. Biol. Macromol.* **2022**, *194*, 1002.
- [25] X. Wang, Q. Liu, S. Wu, B. Xu, H. Xu, *Adv. Mater.* **2019**, *31*, 1807716.
- [26] M. Jin, Z. Wu, F. Guan, D. Zhang, B. Wang, N. Sheng, X. Qu, L. Deng, S. Chen, Y. Chen, H. Wang, *ACS Appl. Mater. Interfaces* **2022**, *14*, 12284.
- [27] J. Z. Ma, Y. Z. Yang, C. Valenzuela, X. Zhang, L. Wang, W. Feng, *Angew. Chem., Int. Edit.* **2022**, *61*, e202116219.
- [28] W. Z. Zou, L. Pattelli, J. Guo, S. J. Yang, M. Yang, N. Zhao, J. Xu, D. S, *Adv. Funct. Mater.* **2019**, *29*, 1808885.
- [29] C. Q. Ye, M. Z. Li, J. P. Hu, Q. F. Cheng, L. Jiang, Y. L. Song, *Environ. Sci.* **2011**, *4*, 3364.
- [30] J. L. Zhao, X. W. Sun, H. Ryu, Y. B. Moon, *Opt. Mater.* **2011**, *33*, 768.
- [31] H. Saito, Y. Neo, T. Matsumoto, M. Tomita, *Opt Express* **2019**, *27*, 28629.
- [32] J. T. Zhu, Y. J. Zhou, B. B. Wang, J. Y. Zheng, S. D. Ji, H. L. Yao, H. J. Luo, P. Jin, *ACS Appl. Mater. Interfaces* **2015**, *7*, 27796.
- [33] A. M. Morsy, M. T. Barako, V. Jankovic, V. D. Wheeler, M. W. Knight, G. T. Papadakis, L. A. Sweatlock, P. W. C. Hon, M. L. Povinelli, *Sci. Rep.* **2020**, *10*, 13964.
- [34] L. Wang, H. K. Bisoyi, Z. G. Zheng, K. G. Gutierrez-Cuevas, G. Singh, S. Kumar, T. J. Bunning, Q. Li, *Mater. Today* **2017**, *20*, 230.
- [35] Q. Q. Yu, M. Guo, W. X. Xu, X. D. Shi, Y. Ma, J. Y. Yu, B. Ding, *Sol. Energy* **2022**, *238*, 9.
- [36] L. Q. Wu, Q. J. Yu, S. Wang, J. Mao, Z. Y. Guo, Y. F. Hu, *J. Mater. Sci.* **2022**, *57*, 12672.
- [37] C. J. Lin, J. Hur, C. Y. H. Chao, G. Z. Liu, S. H. Yao, W. H. Li, B. L, *Sci. Adv.* **2022**, *8*, eabn7359.
- [38] D. Stuart-Fox, A. Moussalli, *PLoS Biol.* **2008**, *6*, e25.
- [39] R. A. Ligon, K. J. McGraw, *Biol. Lett.* **2013**, *9*, 20130892.
- [40] Z. Wang, W. Wang, M. Wamsley, D. Zhang, H. Wang, *ACS Appl. Mater. Interfaces* **2022**, *14*, 17560.
- [41] S. Q. Xiong, Y. Wang, J. R. Yu, L. Chen, J. Zhu, Z. M. Hu, *J. Mater. Chem. A* **2014**, *2*, 7578.
- [42] M. d'Ischia, A. Napolitano, A. Pezzella, P. Meredith, T. Sarn, *Angew. Chem., Int. Ed.* **2009**, *48*, 3914.
- [43] Y. Guo, A. Baschieri, F. Mollica, L. Valgimigli, J. Cedrowski, G. Litwinienko, R. Amorati, *Angew. Chem., Int. Ed.* **2021**, *60*, 15220.
- [44] P. Yang, Z. Gu, F. Zhu, Y. Li, *CCS Chem.* **2020**, *2*, 128.
- [45] L. Han, Y. Zhang, X. Lu, K. Wang, Z. Wang, H. Zhang, *ACS Appl. Mater. Interfaces* **2016**, *8*, 29088.

- [46] Y. Zou, X. Chen, P. Yang, G. Liang, Y. Yang, Z. Gu, Y. Li, *Sci. Adv.* **2020**, 6, eabb4696.
- [47] M. M. Jastrzebska, H. Isotalo, J. Paloheimo, H. Stubb, *J. Biomater. Sci., Polym. Ed.* **1995**, 7, 577.
- [48] W. Cheng, X. Zeng, H. Chen, Z. Li, W. Zeng, L. Mei, Y. Zhao, *ACS Nano* **2019**, 13, 8537.
- [49] J. Qiu, Y. Shi, Y. Xia, *Adv. Mater.* **2021**, 33, 2104729.
- [50] B. Xue, J. Gu, L. Li, W. Yu, S. Yin, M. Qin, Q. Jiang, W. Wang, Y. Cao, *Nat. Commun.* **2021**, 12, 7156.
- [51] Y. H. Ding, M. Floren, W. Tan, *Biosurf. Biotribol.* **2016**, 2, 121.
- [52] P. Kord Forooshani, B. P. Lee, *J. Polym. Sci. A: Polym. Chem* **2017**, 55, 9.
- [53] D. Han, Y. Wang, C. Yang, H. Lee, *ACS Appl. Mater. Interfaces* **2021**, 13, 12735.
- [54] Y. Wu, K. Wang, S. Huang, C. Yang, M. Wang, *ACS Appl. Mater. Interfaces* **2017**, 9, 13602.
- [55] Y. Gao, J. J. Chen, X. Y. Han, Y. D. Pan, P. Y. Wang, T. J. Wang, T. Q. Lu, *Adv. Funct. Mater.* **2020**, 30, 2003207.
- [56] R. Liu, L. Cui, H. Wang, Q. Chen, Y. Guan, Y. Zhang, *ACS Appl. Mater. Interfaces* **2021**, 13, 42052.
- [57] H. Feinberg, T. W. Hanks, *Polym. Int.* **2022**, 71, 578.
- [58] M. Liang, C. He, J. Dai, P. Ren, Y. Fu, F. Wang, X. Ge, T. Zhang, Z. Lu, *J. Mater. Chem. B* **2020**, 8, 8232.
- [59] Y. Liu, K. Ai, J. Liu, M. Deng, Y. He, L. Lu, *Adv. Mater.* **2013**, 25, 1353.
- [60] L. Zong, M. J. Li, C. X. L, *Nano Energy* **2018**, 50, 308.
- [61] Y. J. Xu, Q. W. Cai, X. X. Yang, Y. Z. Zuo, H. Song, Z. M. Liu, Y. P. Hang, *Sol. Energy Mat. Sol. C* **2012**, 107, 316.